Inorganic Chemistry
Article
Cite This: Inorg. Chem. XXXX, XXX, XXX−XXX
pubs.acs.org/IC

Experimental and Theoretical Comparison of Transition-Metal and Actinide Tetravalent Schiff Base Coordination Complexes

Bonnie E. Klamm, Cory J. Windorff, Cristian Celis-Barros, Matthew L. Marsh, David S. Meeker, and Thomas E. Albrecht-Schmitt*

Department of Chemistry and Biochemistry, Florida State University, 95 Chieftan Way, RM. 118 DLC, Tallahassee, Florida 32306, United States

Supporting Information

ABSTRACT: A series of homoleptic tetravalent transition-metal and actinide Schiff-base coordination complexes, ML_2 {M = Zr, Hf, Th, U; L = *N*,*N*′-bis[(4,4′-diethylamino)salicylidene]-1,2-phenylenediamine}, have been synthesized that feature a rigid phenyl backbone. These complexes create the opportunity for comparing a series of complexes containing metal cations in the formal IV+ oxidation state by structural, spectroscopic, and theoretical analysis that also incorporate the previously reported Ce(IV) and Pu(IV) analogues. X-ray crystallographic analysis reveals that all complexes are isomorphous and feature a co-facial ligand geometry. TD-DFT and other quantum mechanical methods were used to explore bonding differences across between the complexes, and resulting calculated absorbance spectra for ML_2 are in good agreement with the experimental data. The computational results also suggest that U(IV) and Pu(IV) analogs have more covalent character in their bonding than found with the other metal cations reported here.

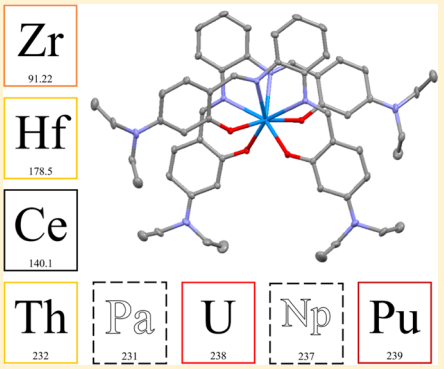

Downloaded from pubs.acs.org by UNIV OF GOTHENBURG on 12/01/18. For personal use only.
Inorg. Chem.

INTRODUCTION

The knowledge and understanding of fundamental actinide bonding trends and coordination modes is significantly limited compared to other elemental series in the periodic table. The lack of actinide studies limits our grasp on the bonding and the electronic structure trends across the 5f series, and how the changes in ligand binding may impact speciation and separation selectivity to different metal ions. There are few comparisons of isostructural molecular complexes in the tetravalent oxidation state. The few studies presented to date are largely limited to comparisons of U(IV) to Th(IV) and comparisons to Pu(IV) are rare.[1−4] Our interest in the chemistry of the early tetravalent actinides is based on the periodic trends through the series. Moving from Th to Pu in: ionic radius, electron configuration, ion acidity, and trends in coordination chemistry and reactivity have been established.[5−12] These elements and their trends provide a way to understand the structural, electronic, and chemical properties of the early actinide elements. In this study, the focus has been placed on the effect of neutral nitrogen donors in the backbone of the ligand as a soft donor. Understanding these bonding differences is important for how they may be utilized for future designs of ligand systems for actinide separations. Of greater interest are the relationships between the actinides, and to the remainder of the periodic table, importantly their tetravalent homologues Zr, Hf, and Ce.[10,11]

Schiff base ligands have been heavily utilized for their ability to stabilize metals in various oxidation states and control the behavior of metals during catalysis.[13] In addition, their steric and electronic properties are highly modular.[14] Salen ligands and their derivatives have been crystallized and characterized with transition metals,[13,15−17] lanthanides,[13,18−22] early actinides (Th and U),[22−28] and very few studies with transuranium elements.[29−33] By utilizing a phenyl-based rigid backbone *N*,*N*′-bis[(4,4′-diethylamino)salicylidene]-1,2-phenylenediamine (H_2L), isolable, crystalline homoleptic compounds of Pu(IV) and Ce(IV) have been studied, eq 1.[33] The rigid

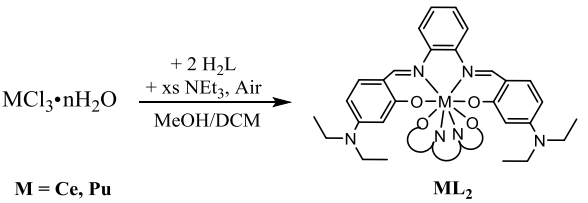

(1)

phenyl backbone gives rises to complexes where the ligands stack in a facial fashion in an 8-coordinate-distorted square antiprismatic geometry. This differs from the dinuclear,[13,18,34] polymeric,[13,18,35] or meridinal[13,36−38] geometries typically observed with other salen complexes because of the small charge to radius of the ion. Complexes PuL_2 and CeL_2 were formed through auto-oxidation in air upon ligation of H_2L in the presence of a base, NEt_3. The UV/vis/NIR properties of the Ce and Pu analogues showed broad, intense charge-transfer

Received: September 21, 2018

© XXXX American Chemical Society

DOI: 10.1021/acs.inorgchem.8b02700
Inorg. Chem. XXXX, XXX, XXX−XXX

bands and ligand-based electrochemical activity. In order to expand this study, we sought to compare the differences between different f-elements and group IV transition-metal complexes by combining synthetic, multinuclear NMR, UV/vis/NIR spectroscopy, and electrochemical and computational work, including comparison and analysis with the Ce and Pu analogues previously synthesized, to offer an electronic structure basis to explain bonding differences.

EXPERIMENTAL SECTION

General Considerations. *Caution! ^{232}Th and ^{238}U isotopes are long-lived, low specific activity α-particle emitting radionuclides and their use presents hazards to human health.*

Materials. Where noted, manipulations were performed with the rigorous exclusion of air and water using glovebox techniques under an argon atmosphere. All air sensitive manipulations were conducted in a negative pressure glovebox dedicated to actinide (^{232}Th−^{249}Cf) chemistry. All manipulations of actinides not inside a glovebox were conducted in a well-ventilated fume hood. THF used for air-sensitive manipulations was purchased anhydrous and stored successively over activated 4 Å molecular sieves two times, and then stored over the sodium metal. Pentane used for air-sensitive manipulations was purchased anhydrous and stored over activated 4 Å molecular sieves. Transition-metal chemistry took place in a routine positive pressure glovebox. THF (Sigma) was sparged with argon, passed through towers containing Q-5 and molecular sieves, and stored over activated 4 Å molecular sieves. $ZrCl_4$ (Sigma) and $HfCl_4$ (Sigma) were used as received and stored in the glovebox. $KN(SiMe_3)_2$ (Sigma) was crystallized from toluene at −35 °C before use and stored in the glovebox. Other solvents used for manipulations in air including MeOH (Sigma), dichloromethane (DCM; Sigma), and pentane (Sigma) were used as received. The following compounds were purchased of reagent grade from commercial sources and were used as received: $Th(NO_3)_4{\cdot}xH_2O$ (Fluka), NEt_3 (Sigma), toluene (VWR), and $CDCl_3$ (Sigma). UCl_4[39] and *N*,*N*′-bis[(4,4′-diethylamino)-salicylidene]-1,2-phenylenediamine ($\mathbf{H_2L}$)[33] were prepared according to the literature.

Instrumentation. Solid-state UV/vis/NIR spectroscopic data were obtained from single crystals using a CRAIC Technologies UV/vis/NIR microspectrophotometer. Crystals were placed on glass slides in immersion oil and data were collected from 300 to 1100 nm. Solution phase UV/vis/NIR data were obtained from 0.08 mM solutions using an Agilent Technologies Cary Series UV−vis−NIR spectrophotometer 6000i. Samples were dissolved in toluene and placed into 1 mm quartz cells. Data were collected from 300 to 1100 nm. ^{1}H and ^{13}C{^{1}H} NMR spectra were recorded on a Bruker 600 MHz spectrometer operating at 600.1 and 150.9 MHz, respectively, at 298 K unless otherwise stated. ^{1}H and ^{13}C{^{1}H} NMR spectra were referenced internally to solvent resonances. NMR samples were removed from the glovebox, dissolved in $CDCl_3$, and placed in an NMR tube with no attempt to exclude air or water. Electrochemical data was recorded on a CH Instruments model 600E Series potentiostat. A three-electrode configuration comprising a platinum disk working electrode (2 mm diameter), a platinum wire counter electrode, and a silver wire pseudoreference electrode were used in all experiments. Cyclic voltammetric scans were conducted in DCM with a 0.1 M $[N^nBu_4][PF_6]$ electrolyte for characterization of the ligand species, $\mathbf{ZrL_2}$, $\mathbf{HfL_2}$, $\mathbf{ThL_2}$, and $\mathbf{UL_2}$ complexes. C/H/N elemental analyses were carried out by Midwest Microlab, Indianapolis, IN, for Zr and Hf samples, and Berkeley Microlab for Th and U samples. Single crystals selected for data collection were mounted on a MITOGEN mount cryoloop and optically aligned on a Bruker D8 Quest X-ray diffractometer. Crystallographic data were collected under a low-temperature nitrogen gas flow using a Mo Kα (λ = 0.71069 Å) X-ray microsource and a CMOS detector. The unit cell determination and subsequent data collection were performed using the APEX III software.[40] Raw data frames were processed using SAINT[41] and SADABS.[42] Subsequent calculations were carried out using the OLEX 2 program.[43] Structures were solved by olex2.solve and refined by full-matrix least-squares on F^2 techniques. Crystal data and other data collection parameters are summarized in Table S4. Crystallographic information files for the complexes are available in the Supporting Information.

Computational Details. The electronic structure and bonding interactions were analyzed using density functional theory (DFT) and time-dependent DFT (TD-DFT). All calculations were carried out using the ORCA 4.0.1.2 package.[44] No geometry optimizations were carried out because the crystallographic molecular structures were available, and the generalized gradient approximation (GGA) and hybrid functionals usually predict geometries very similar to the experimental data. Absorption spectra and excited states were calculated by TD-DFT using GGA functional BP86. Other well-known functionals such as CAM-B3LYP and PBE0 were tested; however, yielded poor experimental resemblance. The def2-TZVP basis set was used for $\mathbf{HfL_2}$. Bonding parameters based on the Bader's theory of quantum theory of atoms in molecules (QTAIM)[45] were calculated and analyzed using the MultiWFN software,[46] and based on wave functions calculated at the PBE0//SARC-TZVP/def2-TZVP level of theory. The electron densities, $\rho(r)$; localization $\lambda(A)$ and delocalization $\delta(A-B)$ indexes; Lagrangian kinetic energies, $G(r)$; potential energy densities, $V(r)$; and total energy densities, $H(r)$; are reported.

Synthesis of $\mathbf{ThL_2}$. In the open atmosphere, $\mathbf{H_2L}$ (17 mg, 0.036 mmol) and NEt_3 (200 μL, 1.43 mmol) in DCM (1 mL) were added to a solution of $Th(NO_3)_4{\cdot}xH_2O$ (10 mg, 0.018 mmol, using the assumption x = 4) in methanol (1 mL). The solution quickly changed from colorless to yellow. Pentane (5 mL) was carefully layered on top of the solution and after 1 d at room temperature, X-ray quality crystals were isolated as yellow columnar crystals, washed with pentane, and dried in air (17 mg, 71% crystalline yield). ^{1}H NMR ($CDCl_3$): δ 8.06 (s, 4H, *H*−C(Ar)═N), 7.04 (m, 4H, Ar-*H*), 6.98 (m, 4H, Ar-*H*), 6.95 (d, $^3J_{HH}$ = 6.95 Hz, 4H, Ar-*H*), 6.02 (dd, $^3J_{HH}$ = 6.02 Hz, 4H, Ar-*H*), 5.73 (s, 4H, Ar-*H*), 3.27 (m, $^2J_{HH}$ = 3.27 Hz, 16H, CH_2), 1.11 (t, $^2J_{HH}$ = 1.11 Hz, 24H, CH_3); ^{13}C{^{1}H} NMR ($CDCl_3$): δ 167.94 (Ar-*C*), 160.32 (Ar-*C*), 153.53 (Ar-*C*), 145.56 (Ar-*C*), 136.00 (Ar-*C*), 125.33 (Ar-*C*), 117.84 (Ar-*C*), 114.54 (Ar-*C*), 102.51 (Ar-*C*), 101.60 (Ar-*C*), 44.38 (CH_2), 13.13 (CH_3). Anal. Calcd for $C_{56}H_{64}N_8O_4Th{\cdot}2CH_2Cl_2$: C, 52.92; H, 5.21; N, 8.52. Found: C, 52.63; H, 5.20; N, 8.52.

Synthesis of $\mathbf{UL_2}$. *Method A.* Inside the glovebox, a vial was charged with UCl_4 (10 mg, 0.026 mmol), capped and removed from the glovebox. In a separate vial, $\mathbf{H_2L}$ (24 mg, 0.053 mmol) and NEt_3 (200 μL, 1.43 mmol) were combined in DCM (1 mL). In a well-ventilated fume hood with no attempt to exclude air or water, the ligand solution was quickly added to UCl_4 in MeOH (1 mL) causing an immediate change from light green to dark red, and then black. Pentane (5 mL) was carefully layered on top of the solution and after 1 d at room temperature, X-ray quality crystals of $\mathbf{UL_2}$ were isolated as red columnar crystals. The crystals were washed with pentane and dried in air (24.0 mg, 69% crystalline yield). Because of the paramagnetism of the U^{4+} ion, only unambiguously identifiable resonances are reported; ^{1}H NMR ($CDCl_3$): δ 10.15 (br, s, $\nu_{1/2}$ = 380 Hz, 2H, Ar-*H*), 7.74 (br, s, $\nu_{1/2}$ = 260 Hz, 4H, Ar-*H*), 3.46 (br, s, $\nu_{1/2}$ = 170 Hz, 8H, Ar-*H*), 2.92 (br, s, $\nu_{1/2}$ = 153 Hz, 8H, Ar-*H*), 1.76 (s, 4H, Ar-*H*), 1.35 (br, m, $\nu_{1/2}$ = 95 Hz, 24H, CH_3), −5.33 (br, s, $\nu_{1/2}$ = 80 Hz, 4H, Ar-*H*); Anal. Calcd for $C_{56}H_{64}N_8O_4U{\cdot}2CH_2Cl_2$: C, 52.69; H, 5.19; N, 8.48. Found: C, 48.32; H, 5.36; N, 8.45. Despite repeated attempts, low carbon content was observed.

Method B. Inside the glovebox, $KN(SiMe_3)_2$ (21 mg, 0.11 mmol) was added to $\mathbf{H_2L}$ (24 mg, 0.053 mmol) in THF (2 mL) quickly causing a change from yellow to red. After 5 min, the ligand solution was added to a pale green solution of UCl_4 (10 mg, 0.026 mmol) in THF (1 mL). The solution quickly changed to dark red with the generation of a gray precipitate (presumably KCl). The mixture was filtered on a glass fiber circle inside a pipette and layered with pentane. After 1 day at ambient glovebox temperature (ca. 23 °C), dark red solids identified as $\mathbf{UL_2}$ (21.5 mg, 60% crystalline yield), as confirmed by ^{1}H NMR spectroscopy, were collected, washed with pentane, and dried under reduced pressure.

DOI: 10.1021/acs.inorgchem.8b02700
Inorg. Chem. XXXX, XXX, XXX−XXX

Synthesis of ZrL_2. As is described in UL_2-method B, $KN(SiMe_3)_2$ (34 mg, 0.17 mmol) was combined with H_2L (39 mg, 0.086 mmol) and added to a solution of $ZrCl_4$ (10 mg, 0.043 mmol), in THF (1 mL) causing an immediate color change to dark orange, identified as ZrL_2 (9.1 mg, 52% crystalline yield). Orange X-ray quality crystals were grown from THF layered with pentane. ^{1}H NMR ($CDCl_3$): δ 8.55 (s, 2H, *H*−C(Ar)═N), 8.05 (s, 2H, Ar-*H*), 7.82 (d, $^3J_{HH}$ = 7.82 Hz, 2H, Ar-*H*), 7.14 (s, 2H, Ar-*H*), 7.08 (d, $^3J_{HH}$ = 7.07 Hz, 2H, Ar-*H*), 6.95 (d, $^3J_{HH}$ = 6.93 Hz, 2H, Ar-*H*), 6.79 (m, 4H, Ar-*H*), 6.04 (d, $^3J_{HH}$ = 6.03 Hz, 2H, Ar-*H*), 5.96 (d, $^3J_{HH}$ = 5.96 Hz, 2H, Ar-*H*), 5.56 (s, 2H, Ar-*H*), 5.11 (s, 2H, Ar-*H*), 3.27 (m, 4H, CH_2), 3.17 (d, $^2J_{HH}$ = 3.18 Hz, 8H, CH_2), 3.11 (m, 4H, CH_2), 1.09 (t, $^2J_{HH}$ = 1.08 Hz, 24H, CH_3); $^{13}C\{^1H\}$ NMR ($CDCl_3$): δ 169.00 (Ar-*C*), 167.11 (Ar-*C*), 166.72 (Ar-*C*), 158.44 (Ar-*C*), 157.41 (Ar-*C*), 153.00 (Ar-*C*), 147.92 (Ar-*C*), 146.93 (Ar-*C*), 134.84 (Ar-*C*), 134.32 (Ar-*C*), 125.45 (Ar-*C*), 124.99 (Ar-*C*), 124.13 (Ar-*C*), 117.96 (Ar-*C*), 116.87 (Ar-*C*), 116.28 (Ar-*C*), 114.57 (Ar-*C*), 114.32 (Ar-*C*), 113.36 (Ar-*C*), 103.09 (Ar-*C*), 102.35 (Ar-*C*), 100.95 (Ar-*C*), 43.94 (CH_2), 13.31 (CH_3). Anal. Calcd for $C_{56}H_{64}N_8O_4Zr{\cdot}0.5OC_4H_8$: C, 66.89; H, 6.59; N, 10.77. Found: C, 62.63; H, 6.29; N, 10.66. Despite repeated attempts, low carbon content was observed.

Synthesis of HfL_2. As is described in UL_2-method B, $KN(SiMe_3)_2$ (25 mg, 0.13 mmol) was combined with H_2L (29 mg, 0.062 mmol) and added to a solution of $HfCl_4$ (10 mg, 0.031 mmol) in THF (1 mL) causing an immediate color change to orange, identified as HfL_2. (15 mg, 22% crystalline yield) Yellow X-ray quality crystals were grown from THF layered with pentane. ^{1}H NMR ($CDCl_3$): δ 8.55 (s, 2H, *H*−C(Ar)═N), 8.07 (s, 2H, Ar-*H*), 7.81 (d, $^3J_{HH}$ = 7.81 Hz, 2H, Ar-*H*), 7.15 (s, 2H, Ar-*H*), 7.05 (d, $^3J_{HH}$ = 7.05 Hz, 2H, Ar-*H*), 6.93 (d, $^3J_{HH}$ = 6.93 Hz, 2H, Ar-*H*), 6.78 (t, $^3J_{HH}$ = 6.78 Hz, 4H, Ar-*H*), 6.02 (d, $^3J_{HH}$ = 6.02 Hz, 2H, Ar-*H*), 5.94 (d, $^3J_{HH}$ = 5.94 Hz, 2H, Ar-*H*), 5.57 (s, 2H, Ar-*H*), 5.12 (s, 2H, Ar−*H*), 3.26 (m, 4H, CH_2), 3.16 (d, $^2J_{HH}$ = 3.18 Hz, 8H, CH_2), 3.12 (m, 4H, CH_2), 1.09 (t, $^2J_{HH}$ = 1.09 Hz, 24H, CH_3); $^{13}C\{^1H\}$ NMR ($CDCl_3$): δ 169.19 (Ar-*C*), 167.53 (Ar-*C*), 166.89 (Ar-*C*), 158.84 (Ar-*C*), 157.75 (Ar-*C*), 153.10 (Ar-*C*), 147.93(Ar-*C*), 146.79 (Ar-*C*), 134.81 (Ar-*C*), 134.23 (Ar-*C*), 125.48 (Ar-*C*), 125.08 (Ar-*C*), 124.19 (Ar-*C*), 118.12 (Ar-*C*), 116.88 (Ar-*C*), 116.37 (Ar-*C*), 114.75 (Ar-*C*), 113.61 (Ar-*C*), 103.12 (Ar-*C*), 102.61 (Ar-*C*), 102.14 (Ar-*C*), 101.37 (Ar-*C*), 44.44 (CH_2), 13.140 (CH_3). We were unable to obtain satisfactory elemental analysis, ^{1}H and $^{13}C\{^1H\}$ NMR spectra of the isolated product is given in Figures S8 and S9.

RESULTS AND DISCUSSION

Synthesis of AnL_2 Complexes (An = Th, U). The tetravalent f-element complexes were prepared in a manner similar to CeL_2 and PuL_2. Briefly, in air, addition of 2 equiv of H_2L in DCM with an excess of triethylamine to a solution of UCl_4 in MeOH results in the formation of an intense dark red/black solution, characteristic of complexation. Layering with pentane yielded X-ray quality crystals overnight, eq 2, Figure 1.

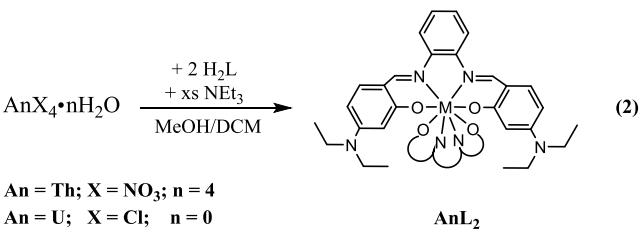

(2)

ThL_2 was prepared in the same manner from $Th(NO_3)_4{\cdot}xH_2O$ (assuming x = 4) and results in an intense yellow solution, layering with pentane-yielded X-ray quality crystals overnight, eq 2, Figure S14. Single-crystal X-ray diffraction studies reveal the structures of both complexes to be isomorphous, with their Ce and Pu analogues and crystallize in the *C*2/*c* space group.[33]

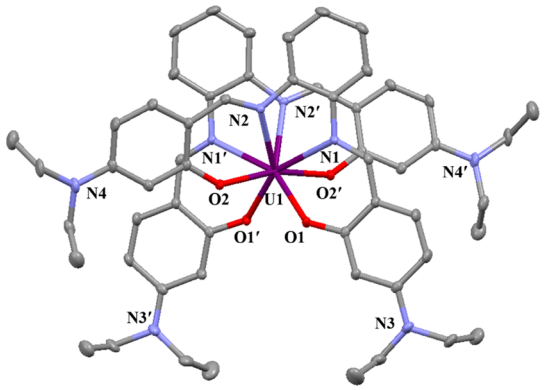

Figure 1. Molecular structure of UL_2 drawn at the 50% probability level with hydrogen atoms and lattice solvent omitted for clarity. The corresponding ThL_2 structure is isomorphous, see the Supporting Information.

As was observed with the Pu and Ce analogues, the complex forms a distorted square antiprismatic geometry with the ligands forming a facial "sandwich" type structure. The ligands bend at a slight 17° from the equatorial plane, typical of these phenyl-substituted backbone Schiff base complexes.[17,47,48]

The average U−O and U−N bond lengths of UL_2 are 2.250(1) and 2.588(2) Å, respectively, and in comparison to other U(IV) Schiff base complexes, Table 1, the U−O bond lengths are significantly longer than the unsubstituted bis salophen complex $U(L^1)_2$[24] and the monosalen complex $U(L^3)Cl_2(Py)_2$;[27] 2.220(1) and 2.190(4) Å, respectively. The U−N bond lengths are similar to the 2.59(2)−2.63(1) Å range reported for other UL_n^x (n = 1, 2) complexes, Table 1. The O(1)−U−O(2) and N(1)−U−N(2) angles for UL_2 are 86.23(5) and 61.09(5)°, respectively. The N(1)−U−N(2) compare well with the 61.11−65.7(2)° range reported for the mono Schiff base complexes $U(L^2)_2$ and $U(L^3)Cl_2(Py)_2$ and the unsubstituted bis salophen complex $U(L^1)_2$; 62.65(15), 65.7(2), 61.11°, respectively, whereas the O(1)−U−O(2) angle is only comparable with $U(L^1)_2$ complex and significantly smaller than the angles reported for $U(L^2)_2$ and $U(L^3)Cl_2(Py)_2$; 154.56(15), 152.2(2)°, respectively.

Table 1. Metrical Comparisons of UL_2 with Other 8-Coordinate U-Schiff Base Complexes[a]

title complex	avg. U−O (Å)	avg. U−N_L (Å)	O−U−O (deg)	N−U−N (deg)
UL_2	2.250(8)	2.588(2)	86.23(5)	61.09(5)
$U(L^1)_2$[24]	2.3(1)	2.62(2)	86.50	61.11
$U(L^2)_2$[23]	2.23(2)	2.60(1)	154.6(2)	62.6(2)
$U(L^3)Cl_2(Py)_2$[27]	2.190(4)	2.59(2)	152.2(2)	65.7(2)

[a]Only distances pertaining to the Schiff base ligand(s) are given. **L** = *N*,*N*′-bis[(4,4′-diethylamino)salicylidene]-1,2-phenylenediamine, R = NEt_2; L^1 = unsubstituted salophen = *N*,*N*′-disalicylidene-*o*-phenylenediaminate, R = H; L^2 = *N*,*N*′-bis(3-methoxysalicylidene)-*o*-phenylenediaminate, R = OCH_3; and L^3 = (±)-*trans*-3,3′-diethoxy-2,2′-[cyclohexane-1,2-diylbis(nitrilomethanylylidene)]diphenol, R = OCH_2CH_3.

The average Th−O bond length in ThL_2 is 2.306(1) Å, which is comparable to other 8-coordinate thorium Schiff base complexes, $Th(L^1)_2$[49] and $Th(L^4)_2$,[22] with average Th−O distances of 2.3(4) and 2.29(3), Å, respectively, and is significantly longer than the mono/bis Th(salophen) com-

DOI: 10.1021/acs.inorgchem.8b02700
Inorg. Chem. XXXX, XXX, XXX−XXX

plexes: $Th(L^5)_2$[26] and $Th(L^3)Cl_2(py)_2$[27] with average Th−O distances of 2.270(1) and 2.21(1), Å, respectively, Table 2,

Table 2. Metrical Comparisons of ThL_2 with Other 8-Coordinate Th-Schiff Base Complexes[a]

title complex	avg. Th−O (Å)	avg. Th−N (Å)	O−Th−O (deg)	N−Th−N (deg)
ThL_2	2.306(1)	2.637(8)	87.40(4)	60.43(4)
$Th(L^1)_2$[49]	2.3(4)	2.65(2)	93.69	60.01
$Th(L^4)_2$[22]	2.29(3)	2.63(1)	83.9(3)	61.4(2)
$Th(L^5)_2$[26]	2.270(1)	2.658(2)		
$Th(L^3)Cl_2(Py)_2$[27]	2.21(1)	2.61(1)	154.1(6)	64.3(6)

[a]Only distances pertaining to the Schiff base ligand(s) are given. **L** = *N*,*N*′-bis[(4,4′-diethylamino)salicylidene]-1,2-phenylenediamine, R = NEt_2; L^1 = salophen = *N*,*N*′-disalicylidene-*o*-phenylenediaminate, R = H; L^4 = 1,1′-{(1*E*,1′*E*)-{[1,2-phenylenebis-(azanylylid-ene)}]bis-(methanylylidene)}bis(naphthalen-2-ol), R = H; L^5 = bis-[*N*,*N*′-bis-(3-allyl salicylidene)-*o*-phenylenediamine], R = $CH_2CH{=}CH_2$; and L^3 = (±)-*trans*-3,3′-diethoxy-2,2′-[cyclohexane-1,2-diylbis-(nitrilomethanylylidene)]diphenol, R = OCH_2CH_3.

whereas the average Th−N bond length of 2.639(1) Å in ThL_2 compares well with the 2.61(1)−2.658(2) Å average Th−N lengths, Table 2. The O(1)−Th−O(2) and N(1)−Th−N(2) angles are 87.40(4) and 60.43(4)°, respectively. Although the O(1)−Th−O(2) angle agrees with the range 83.9(3)−93.69°, the monosalen complex $Th(L^3)Cl_2(Py)_2$[27] is significantly different, 154.1(6)°, Table 2, and the N(1)−Th−N(2) angle compares well with the range 60.01−64.3(6)° reported for other Th(salen) complexes.

Synthesis of ML_2 Complexes (M = Hf, Zr, U). Because of the sensitivity of $HfCl_4$ and $ZrCl_4$ to moisture, HfL_2 and ZrL_2 were synthesized inside a glovebox. Additionally, the uranium analogue was synthesized in a glovebox for comparison with its synthesis in air to confirm that no oxidation was taking place. Briefly, in situ deprotonation of H_2L with $KN(SiMe_3)_2$ in THF quickly caused a color change from yellow to red-orange, addition of this solution to MCl_4 in THF caused a color change to orange for Zr, yellow for Hf, and dark red for U. Filtration followed by layering with pentane at ambient glovebox temperature (ca. 23 °C) gave X-ray quality crystals after one day for ZrL_2 and HfL_2, eq 3, Figure 2, UL_2 was confirmed by ^1H NMR analysis.

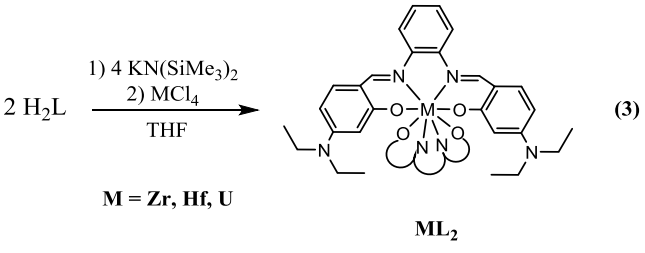

(3)

ZrL_2 and HfL_2 are isomorphous with one another and crystallize with two independent units in the $P2_1/c$ space group. The average Zr−O and Zr−N bond lengths of ZrL_2 are 2.113(2) and 2.375(2) Å, respectively, and in comparison to other Zr(IV) Schiff base complexes. The Zr−O bond lengths are slightly longer than the bis salophen complexes $Zr(L^6)_2$[17] and $Zr(L^7)_2$;[50] 2.109(5) and 2.085(5) Å respectively, see Table 3. The Zr−N bond lengths are slightly shorter than the 2.40(2)−2.42(1) Å range reported for other $Zr(L^x)_2$ complexes, Table 3. The average O−Zr−O and N−Zr−N

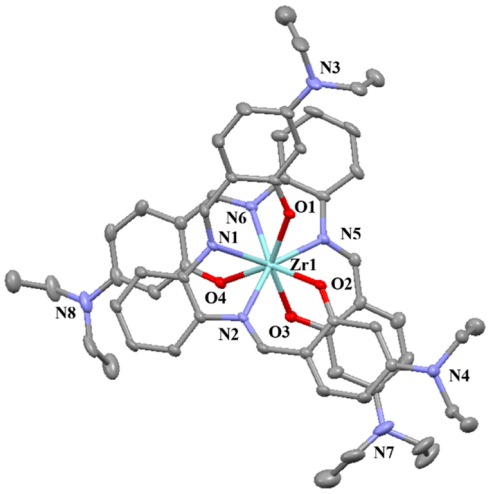

Figure 2. Thermal ellipsoid plot of one of the two crystallographic independent units of ZrL_2 drawn at the 50% probability level with hydrogen atoms, disorder, and lattice solvent omitted for clarity. The HfL_2 compound is isomorphous, see the Supporting Information.

Table 3. Metrical Comparisons of HfL_2 and ZrL_2 with Other 8-Coordinate Zr-Salophen Complexes[a]

title complex	avg. M−O (Å)	avg. M−N (Å)	O−M−O (deg)	N−M−N (deg)
HfL_2	2.108(2)	2.358(3)	74.29(8)	66.54(9)
ZrL_2	2.113(2)	2.375(2)	74.73(7)	66.21(8)
$Zr(L^6)_2$[17]	2.109(5)	2.40(2)	74.25(7)	66.21
$Zr(L^7)_2$[50]	2.085(5)	2.42(1)	96.5(2)	67.2(4)

[a]Only distances pertaining to the Schiff base ligand(s) are given. **L** = *N*,*N*′-bis[(4,4′-diethylamino)salicylidene]-1,2-phenylenediamine, R = NEt_2; L^6 = (5-methoxysalicylidene)-4,5-dimethyl-1,2-phenylenediamine, R = OCH_3; and L^7 = bis(4-amino-*N*,*N*′-disalicylidene-l,2-phenylenediaminato), R = H.

angles for ZrL_2 are 74.73(7) and 66.21(8)°, respectively. The N−Zr−N angles compare well with both of the salophen complexes $Zr(L^6)_2$[17] and $Zr(L^7)_2$;[50] 66.21 and 67.2(4)°, respectively, whereas O−Zr−O is only comparable with the $Zr(L^6)_2$[17] complex and significantly smaller than the angle reported for $Zr(L^7)_2$;[50] 74.25(7) and 96.5(2)°, respectively.

The Hf−O and H−N average bond lengths in HfL_2 are 2.108(2) and 2.358(3) Å, respectively. For hafnium, there are only two other 7-coordinate crystallographically characterized complexes with salen-like Schiff base ligands, both complexes feature a saturated cyclohexyl backbone rather than a rigid phenyl ring, namely, $Hf_2O_2(L^8)_2(OBu^t)_2$ [L^8 = *N*,*N*′-bis(3,5-di-*t*-butylsalicylidene)-1,2-cyclohexanediamine][51] and $Hf(L^9)(OPh)_2(H_2O)$ {L^9 = [1,1′-binaphthalen]-2-ol, 3,3″-[(1*R*,2*R*)-1,2-cyclohexanediylbis[(*E*)-nitrilomethylidyne]]bis-(1*R*,1″*R*), R = napthalene}[52] which have relevant Hf−O and Hf−N average bond distances of 2.099(4), 2.35(3) and 2.06(1), 2.35(1) Å, respectively. Although Hf−O bond lengths are similar to the Zr analogue, the Hf−N bonds are significantly smaller. The average O−Hf−O and N−Hf−N bond angles are 74.2(6) and 66.5(5)°, respectively. The two ligands coordinating to Hf and Zr are rotated 143.2° and 143.8° from each other, respectively, and are significantly bent from the central plane by a difference of 20°. The ligands on Hf and Zr exhibit a bend of ∼10° on one side and ∼30° on the other. These parameters are significantly different from Th, U, and reported Ce and Pu structures.[33]

DOI: 10.1021/acs.inorgchem.8b02700
Inorg. Chem. XXXX, XXX, XXX−XXX

Table 4. Metrical Comparisons of Average Selected Bond Distances (Å) and Angles (deg) for ML_2 (M = Zr, Hf, Ce, Th, U, Pu) Complexes

complex	8-coordinate ionic radius[53]	M−O_{avg} (Å)	M−N_{avg} (Å)	O−M−O (deg)	N−M−N (deg)
HfL_2	0.83	2.108(2)	2.358(3)	74.29(8)[a]	66.54(9)[a]
ZrL_2	0.84	2.113(2)	2.375(2)	74.73(7)[a]	66.21(8)[a]
PuL_2[33]	0.96	2.225(1)	2.555(3)	84.9(1)	61.6(1)
CeL_2[33]	0.97	2.240(2)	2.590(2)	85.82(6)	61.09(6)
UL_2	1.0	2.250(8)	2.588(2)	86.23(5)	61.09(5)
ThL_2	1.05	2.306(1)	2.639(1)	87.40(4)	60.43(4)

[a]Average bond angles.

The homoleptic nature of the reported ML_2 (M = Zr, Hf, Ce, Th, U, Pu) complexes allow for a rare direct comparison of solid-state metrical parameters between Ce, Th, U, and Pu.[1−3,7,11] The average M−O and M−N bond distances, and the O(1)−M−O(2) and N(1)−M−N(2) angles are listed in Table 4. The O−M−O angles are periodic with the largest for ThL_2, 87.40(4)° and smallest for PuL_2, 84.9(1)°, whereas the N(1)−M−N(2) bond angle follows the opposite trend with PuL_2 having the greatest angle 61.6(2)° and ThL_2 with the smallest angle 60.43(4)°. The rotation of the two overlapping salophen ligands for complexes AnL_2 [calculated from the average value of torsion angles between O(1)···O(2)^O(1′)···O(2′) and N(1)···N(2)^N(1′)···N(2′)] is largest for ThL_2 50.4° and smallest for PuL_2 49.5°.

To summarize, a crystallographic comparison across several ML_2 complexes shows that the transition metal compounds ZrL_2 and HfL_2 have similar bond and angle metrics and are significantly shorter than their f-element analogues. However, amongst the f-element complexes, only ThL_2 features bond distances that are significantly longer than another f-element complexes, likely due to the larger ionic radius of the Th^{4+} ion (1.05 Å, 8-coordinate[53]). All of the O−M−O and N−M−N for the f-elements are distinct from one another and from the transition-metal complexes. Figure 3 depicts these comparisons in graphical form by showing the near linear relationship between mean M−O and M−N bond distances and metal ionic radii.

Spectroscopy and Electrochemistry of ML_2. *^1H and ^{13}C NMR Spectroscopy.* The complexes reported ZrL_2, HfL_2, and ThL_2 are all diamagnetic and give typical ^1H and $^{13}C\{^1H\}$ NMR shifts in $CDCl_3$, with the notable exceptions that because of the small ionic radii of Zr and Hf, the aromatic protons become unique between the two ligands rather than symmetric as is observed in the ThL_2 and CeL_2 complexes.[33] Additionally in all diamagnetic complexes, some stereochemical uniqueness is observed in the methylene unit of the $-N(CH_2CH_3)_2$ substituent giving rise to multiple resonances such as ZrL_2, where there are three resonances in 4:8:4 integration, or in ThL_2, where a multiplet of 10 is observed with the expected integration of 16. The paramagnetic U^{4+} ion in UL_2 gave a typical paramagnetic spectrum with several broad signals in the range of +11 to −6 ppm, with only unambiguously identifiable peaks being assigned.

UV/vis/NIR Spectroscopy. Solution UV/vis/NIR spectroscopy of ML_2 (M = Zr, Hf, Ce, Th, U) in toluene reveals an intense broad band with λ_{max} in the range of 367−384 nm, with ε values in the range of 190 000−240 000 (L mol^{-1} cm^{-1}), Figure 4. Despite attempts to measure more concentrated solutions, no 5f → 5f peaks were observed for UL_2. Solid-state UV/vis/NIR spectra of ML_2 (M = Zr, Hf, Ce, Th, U, Pu), Figure 5, reveal an intense broad band with λ_{max} at 491, 483, 411, 462, 546, and 529 nm, respectively. This intense, broad feature is characteristic of ML_2 complexes, accounting for the intense coloring of each crystal. TD-DFT calculations attribute these strong absorptions to ligand-to-metal charge transfer (LMCT) for ML_2, with additional metal-to-ligand charge transfer (MLCT) excitations in UL_2 that account for its low-energy charge-transfer band. For the UL_2 and PuL_2 complexes, see below. The weak absorptions between 700 and 1100 nm for An(IV) are assigned to Laporte-forbidden 5f → 5f transitions, characteristic of the tetravalent state.[54,55]

Electrochemistry of ML_2. To further investigate the tetravalent series, the redox potentials of ML_2 were measured via cyclic voltammetry in nonaqueous solution to compare

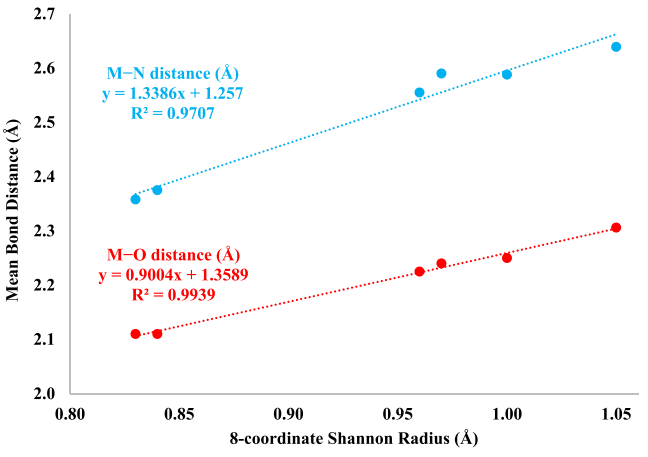

Figure 3. Plot of the mean M−N (blue) and M−O (red) bond distances (Å) in ML_2 (M = Zr, Hf, Ce, Th, U, Pu) relative to the ionic radius of M.[53] 3σ error bars calculated from the standard deviation in the mean distance of M−N and M−O bonds.

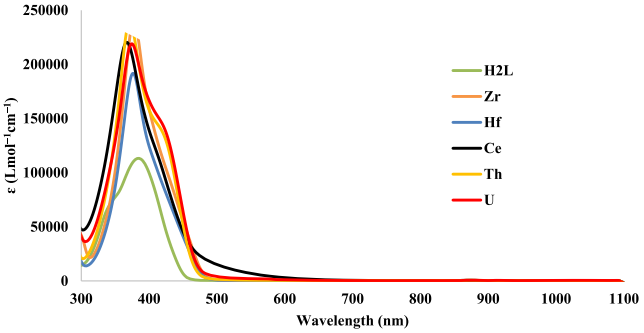

Figure 4. Solution phase UV/vis/NIR absorption spectra of ML_2 (M = Zr, Hf, Ce, Th, U) in toluene at 298 K.

DOI: 10.1021/acs.inorgchem.8b02700
Inorg. Chem. XXXX, XXX, XXX−XXX

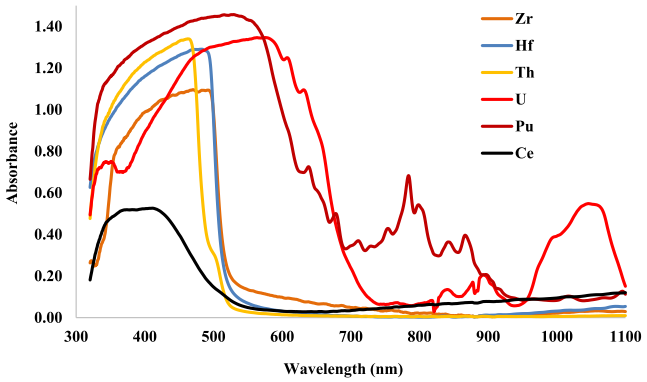

Figure 5. Solid-state UV/vis/NIR absorbance spectra of $\mathbf{ML_2}$ (M = Zr, Hf, Ce, Th, U, Pu).

with the previously reported $\mathbf{CeL_2}$ and $\mathbf{PuL_2}$.[33] As observed in the previous study, the ligand is redox active and exhibits reversible or quasireversible behavior, primarily reduction, that is, altered by the Lewis acidity of the metal, Figure S5.

The ligand is noted to have several oxidation and reduction peaks. The reductive capacity of the plain salophen ligand has been explored in the $\mathbf{UL^1_2}$[24] complex, which showed that chemical addition of $2e^-$ caused ligand reduction and coupling displaying the reduction potential of the unsubstituted salophen ligand ($E_{1/2}$ = −1.14 V vs Fc^+/Fc)[24,28] to be less than the generic $U^{4+/3+}$ potential of −0.12 V versus Fc^+/Fc.[56] However, in this study, it has been observed that the first major anodic peak gives the best comparisons between the different $\mathbf{ML_2}$ complexes. The oxidation peaks, which occur between 0.08 and 0.486 V potentials, can be plotted against the 8-coordinate ionic radii, see Figure 6. As the ionic radius

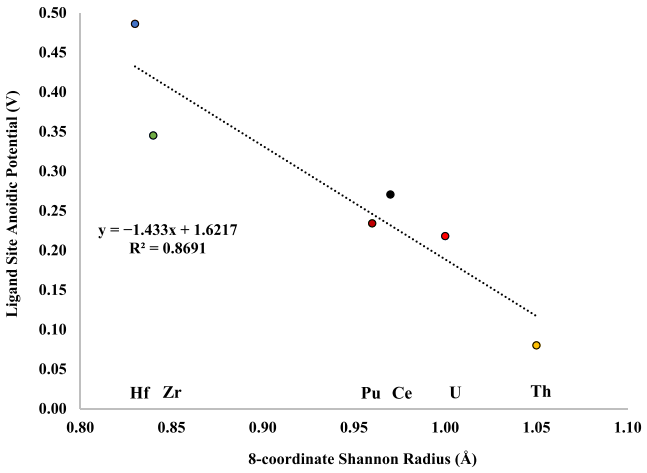

Figure 6. Tetravalent 8-coordinate Shannon radii plotted against the respective common ligand site oxidation potentials for $\mathbf{ML_2}$ (M = Zr, Hf, Ce, Th, U, Pu).

increases, the oxidation potential decreases, that is, becomes less positive and gives a good linear fit across all $\mathbf{ML_2}$ complexes (M = Zr, Hf, Ce, Th, U, Pu). The calculated potential stabilization because of reduction in ionic radii from this plot is derived to be 140 mV/Å.

Theoretical Analysis. *Time-Dependent DFT.* The excited states of $\mathbf{ML_2}$ (M = Zr, Hf, Ce, Th, U, Pu) complexes were calculated by TD-DFT to understand similarities and differences between their electronic structures. Although DFT fails to describe static correlation properly because the theory is based on total density rather than individual electrons,[57] it remains the best option for closed shell systems because of its computational costs and accuracy. Open-shell systems are more difficult to treat because of their sensitivity to electron correlation and multiconfigurational methods are highly recommended. In this study, $\mathbf{UL_2}$ and $\mathbf{PuL_2}$ were analyzed together as open-shell sets, where complete active space self-consistent field (CASSCF) was unsuccessfully applied. When calculations were performed on the full molecule in CASSCF, the calculations failed to converge. Thus, DFT is a good alternative for insight on the nature of the electronic structure of $\mathbf{UL_2}$ and $\mathbf{PuL_2}$.

The calculated absorption spectra of $\mathbf{UL_2}$ and $\mathbf{PuL_2}$ are characterized by low-intensity bands at low energies that correspond to predominantly f → f transitions, Figure 7. These transitions are not well reproduced (peak 3a) because of the inability of DFT to include spin−orbit coupling. Additionally, the strong mixing between the actinide 5f and ligand 2p orbitals produce variation in the nature of these transitions between $\mathbf{UL_2}$ and $\mathbf{PuL_2}$ (Table S1). This mixing is also responsible for the broad band feature observed around 450 nm, which is assigned as LMCT for both U(IV) and Pu(IV), with some additional MLCT transitions in the U(IV) broad band. Figure 8 shows the three types of orbitals involved in these transitions, where strongly mixed orbitals are represented as $f\pi$ (Figure 8b).

In comparison, the closed shell $\mathbf{ML_2}$ (M = Zr, Hf, Ce, Th) systems are characterized mainly by $\pi \rightarrow \pi^*$ and LMCT transitions that are responsible for the high intensity of the transitions in the TD-DFT spectra, Figure S13. The band intensity for $\mathbf{CeL_2}$ is significantly decreased in both the experiment and theory that could be attributed to the dominating $\pi \rightarrow$ f and $\pi \rightarrow f\pi$ transitions, Table S2. The $4f-\pi^*$ orbital mixing is an important factor in terms of the electronic structure of the closed shell complexes. This can also be seen in the excited states of $\mathbf{CeL_2}$, Table S2b,c, where virtual bonding molecular orbitals that are formed by the mixture of unoccupied ligand orbitals and 4f Ce orbitals, are populated. These transitions are not seen in the isoelectronic actinide analogue, $\mathbf{ThL_2}$.

Quantum Theory of Atoms in Molecules. Bader's theory[45] has been a useful tool to analyze the nature of bonding in molecules by not only analyzing its electron density (ρ) but also relating it with its energy. This specific term called the energy density (H) is referred to as the sum of potential energy (V) and Lagrangian kinetic energy (G).[58] Because of crystallographic symmetry, the $\mathbf{ML_2}$ (M = Ce, Th, U, Pu) asymmetric unit contains only one ligand. The M−O(1) and M−O(2) bonds are significantly different for $\mathbf{UL_2}$ [2.258(1), 2.241(1) Å], and the M−N(1) and M−N(2) bonds are significantly different for $\mathbf{ML_2}$ (M = Ce, Th, U, Pu) by 0.024, 0.017, 0.020, and 0.028 Å, respectively, Tables 5 and S3, and can be compared in terms of the electron and total energy density, Figure 9. The M−O bond critical points (BCPs) have an increased accumulation of electron density over the M−N bonds. In addition, the increased electron density at the M−O BCP is accompanied by more negative values of the total energy density, related to the increased covalency character of M−O over M−N bonds.

Hf(IV) differs from f-block metals by differential bonding parameters, in that it is able to bind more covalently to nitrogen atoms. The decrease in energy density in the Hf−O

DOI: 10.1021/acs.inorgchem.8b02700
Inorg. Chem. XXXX, XXX, XXX−XXX

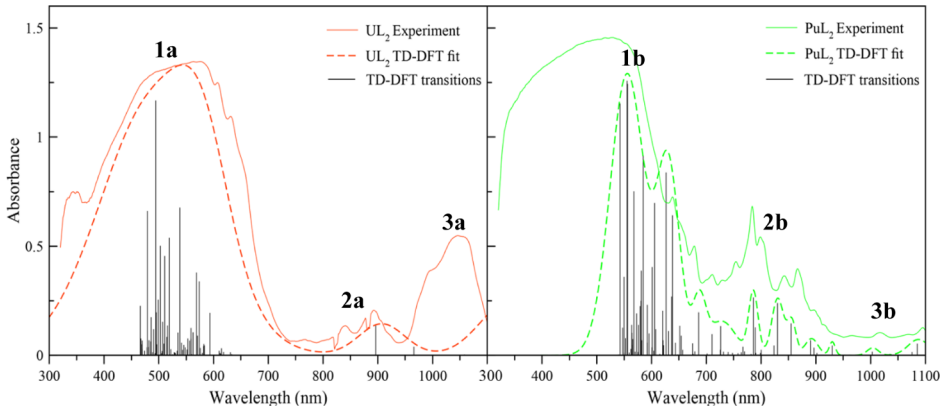

Figure 7. Calculated TD-DFT UV/vis/NIR absorption spectra of $\mathbf{UL_2}$ (left) and $\mathbf{PuL_2}$ (right). Solid and dashed lines correspond to the experimental and Gaussian fit of the calculated transitions, respectively. The oscillator strength for $\mathbf{UL_2}$ and $\mathbf{PuL_2}$ was scaled up to 20 and 35%, respectively. Labeled peaks correspond to transition assignments described in Table S1.

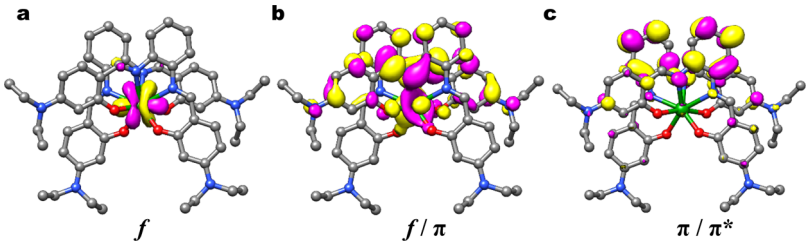

Figure 8. DFT-orbitals involved in the TD-DFT absorption spectrum with hydrogen atoms omitted for clarity. (a) Non-bonding 5f-orbitals, (b) strongly mixed 5f-metal−π-ligand orbitals (c) π- and π*-ligand orbitals.

Table 5. Bonding Metrics Derived from the QTAIM Theory[a]

	$\rho(r)$	$\lvert V(r)\rvert/G(r)$	$H(r)$	$H(r)/\rho(r)$
Hf−O(avg)	0.0905	1.1413	−0.0162	−0.1793
Ce−O(2)	0.0856	1.1856	−0.0163	−0.1905
Th−O(1)	0.0805	1.1853	−0.0152	−0.1881
U−O(2)	0.0907	1.1860	−0.0180	−0.1990
Pu−O(2)	0.0914	1.1724	−0.0181	−0.1980
Hf−N(avg)	0.0625	1.1807	−0.0104	−0.1662
Ce−N(1)	0.0487	1.1026	−0.0038	−0.0782
Th−N(2)	0.0488	1.1560	−0.0056	−0.1142
U−N(1)	0.0529	1.1476	−0.0060	−0.1126
Pu−N(2)	0.0531	1.1254	−0.0056	−0.1053

[a]M−O and M−N data correspond to the stronger bonds for each oxygen and nitrogen bond.

bonds could also be understood as a less pronounced preference for hard donor ligands. Ce(IV) and Th(IV) present subtle differences which are seen in the decreased electron density in Th−O BCPs, and less negative energy densities that argue in favor of the increased covalent character of Ce(IV). U(IV) and Pu(IV) also present similar bonding parameters; however, differ from the other metals by the increased electron density and enhanced energy densities that agree with the well-known covalent character of these metals. Although Pu(IV) seems to be more covalent by the increased overlap in the molecular orbitals, this is recognized as the overestimation of correlation in DFT.[2]

The $V(r)/G(r)$ ratio is useful to see the degree of predominance of the potential energy over the kinetic energy, that is, for $\lvert V(r)\rvert/G(r) > 1$, the interaction is stabilized by a local concentration of the charge.[59] This also can be understood as the stabilization of the electron density at the

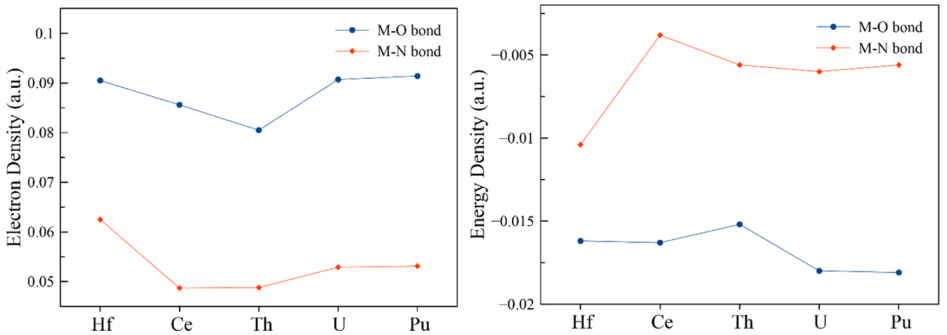

Figure 9. Electron (left) and total energy (right) density parameters in the M−O and M−N BCPs in $\mathbf{ML_2}$ (M = Hf, Ce, Th, U, Pu). All parameters were calculated from their corresponding DFT wave functions. Numerical data are found in the Supporting Information.

DOI: 10.1021/acs.inorgchem.8b02700
Inorg. Chem. XXXX, XXX, XXX−XXX

BCP produced by an increased potential energy and/or a reduction of the kinetic energy of these electrons. According to Table 5, the energy of the M−O bonds are in the range of 17−18% of potential energy predominance except for Hf−O that is reduced to 14%. However, the Hf−N bonds present 18% of predominance being the highest percentage with respect to the M−N bonds. This explains why Hf bonds are similar in terms of the covalent character as previously mentioned. Additionally, Ce/Th differences can be seen more clearly in M−N bonds, where Th(IV) shows around 6% of increased predominance of the potential energy with respect to the isoelectronic Ce(IV). Thus, Ce differs from Th in how they bind to softer donor ligands rather than hard donor ligands.

Because of the scarcity of reported bonding parameters for these tetravalent metals, it is difficult to compare with other complexes. There are few studies that report the electron densities, Laplacian of the electron density, and integrated parameters for tetravalent lanthanide/actinide systems.[60−62] Although the best way to compare bonding parameters between complexes is to compare their normalized energy densities (H/ρ), none have been reported. Electron densities have been reported for other coordination complexes; however, these are not directly comparable as the electron density localized in the BCP decreases with increasing coordination number. In another study, where the 5-coordinate **M(BIPM^{TMS})(ODipp)$_2$**, [M = Ce, Th, U; BIPM^{TMS} = C(PPh$_2$NSiMe$_3$)$_2$; Dipp = C$_6$H$_3$-2,6-^{i}Pr$_2$] complexes were examined, the total electron densities of Ce(IV), Th(IV), and U(IV) were reported to be 0.4008, 0.3989, and 0.4568 au, respectively.[62] However, the study on **M(BIPM^{TMS})(ODipp)$_2$** examined metals in a lower coordination environment that feature an unusual M═C bonding interaction, and used a higher level of theory in terms of electron correlation. Therefore, these reported values are not completely comparable and should be considered carefully. In the 8-coordinate **ML$_2$** complexes reported here, the calculated electron densities of Ce(IV), Th(IV), and U(IV) are 0.5294, 0.5125, and 0.5631 au, respectively. Although the values reported here suggest a higher degree of covalency for **ML$_2$** over the previously reported **M(BIPM^{TMS})(ODipp)$_2$** complexes, they need to be confirmed using a more correlated wave function.

CONCLUSIONS

Herein, we have structurally characterized a series of tetravalent transition (Zr and Hf) and actinide (Th and U) metal complexes with the Schiff base ligand, **H$_2$L** {**L** = *N*,*N*′-bis[(4,4′-diethylamino)salicylidene]-1,2-phenylenediamine} in the form of **ML$_2$**, analogous with the previously reported **CeL$_2$** and **PuL$_2$** complexes. The **ML$_2$** family of complexes allows for a comparison across a series of elements by various spectroscopic and theoretical techniques. Crystallographic analysis finds that the bonding trends follow the ionic radii of the elements with **ThL$_2$** showing the longest bond lengths, whereas **HfL$_2$** shows the shortest bond lengths. The absorbance spectra of all **ML$_2$** complexes show intense, broad MLCT bands with several f → f peaks in the **UL$_2$** and **PuL$_2$** spectra, in the solid state, which were successfully modeled by TD-DFT. Comparison of **UL$_2$** and **PuL$_2$** reveal similar bonding parameters, whereas **CeL$_2$** shows increased covalent behavior compared to **ThL$_2$**. The ligand−metal overlap is also clearly enhanced in **UL$_2$** and **PuL$_2$**.

ASSOCIATED CONTENT

Supporting Information

The Supporting Information is available free of charge on the ACS Publications website at DOI: 10.1021/acs.inorgchem.8b02700.

Photographs of compounds, NMR spectra, electrochemical data, crystallographic data collection, structure solution, refinement, and X-ray diffraction details of compounds **ZrL$_2$**, **HfL$_2$**, **ThL$_2$**, and **UL$_2$** (CIF, CCDC no. 1868460-63) (PDF)

Accession Codes

CCDC 1868460−1868463 contain the supplementary crystallographic data for this paper. These data can be obtained free of charge via www.ccdc.cam.ac.uk/data_request/cif, or by emailing data_request@ccdc.cam.ac.uk, or by contacting The Cambridge Crystallographic Data Centre, 12 Union Road, Cambridge CB2 1EZ, UK; fax: +44 1223 336033.

AUTHOR INFORMATION

Corresponding Author

*E-mail: talbrechtschmitt@fsu.edu.

ORCID

Bonnie E. Klamm: 0000-0002-1168-0932
Cory J. Windorff: 0000-0002-5208-9129
Cristian Celis-Barros: 0000-0002-4685-5229
Thomas E. Albrecht-Schmitt: 0000-0002-2989-3311

Notes

The authors declare no competing financial interest.

ACKNOWLEDGMENTS

We thank the Chemical Sciences, Geosciences, and Biosciences Division of the Office of Basic Energy Sciences of the Department of Energy for supporting the research as part of the Center for Actinide Science and Technology (CAST) funded by the U.S. Department of Energy, Office of Science, Office of Basic Energy Sciences, under Award Number DE-SC0016568. The authors also acknowledge computational support from the Universidad Andres Bello, Santiago, Chile, through the FONDECYT grant no. 1180017.

REFERENCES

(1) Gaunt, A. J.; Reilly, S. D.; Enriquez, A. E.; Scott, B. L.; Ibers, J. A.; Sekar, P.; Ingram, K. I. M.; Kaltsoyannis, N.; Neu, M. P. Experimental and Theoretical Comparison of Actinide and Lanthanide Bonding in M[N(EPR$_2$)$_2$]$_3$ Complexes (M = U, Pu, La, Ce; E = S, Se, Te; R = Ph, iPr, H). *Inorg. Chem.* **2008**, *47*, 29−41.

(2) Schnaars, D. D.; Gaunt, A. J.; Hayton, T. W.; Jones, M. B.; Kirker, I.; Kaltsoyannis, N.; May, I.; Reilly, S. D.; Scott, B. L.; Wu, G. Bonding Trends Traversing the Tetravalent Actinide Series: Synthesis, Structural, and Computational Analysis of An^{IV}(Aracnac)$_4$ Complexes (An = Th, U, Np, Pu; Aracnac = ArNC(Ph)CHC(Ph)O; Ar = 3,5-tBu$_2$C$_6$H$_3$). *Inorg. Chem.* **2012**, *51*, 8557−8566.

(3) Jones, M. B.; Gaunt, A. J.; Gordon, J. C.; Kaltsoyannis, N.; Neu, M. P.; Scott, B. L. Uncovering f-element bonding differences and electronic structure in a series of 1:3 and 1:4 complexes with a diselenophosphinate ligand. *Chem. Sci.* **2013**, *4*, 1189−1203.

(4) Löble, M. W.; Keith, J. M.; Altman, A. B.; Stieber, S. C. E.; Batista, E. R.; Boland, K. S.; Conradson, S. D.; Clark, D. L.; Lezama Pacheco, J.; Kozimor, S. A.; Martin, R. L.; Minasian, S. G.; Olson, A. C.; Scott, B. L.; Shuh, D. K.; Tyliszczak, T.; Wilkerson, M. P.; Zehnder, R. A. Covalency in Lanthanides. An X-ray Absorption Spectroscopy and Density Functional Theory Study of LnCl$_6^{x-}$ (x = 3, 2). *J. Am. Chem. Soc.* **2015**, *137*, 2506−2523.

DOI: 10.1021/acs.inorgchem.8b02700
Inorg. Chem. XXXX, XXX, XXX−XXX

(5) Clark, D. L.; Hobart, D. E.; Neu, M. P. Actinide Carbonte Complexes and Their Importance in Actinide Environmental Chemistry. *Chem. Rev.* **1995**, *95*, 25−48.
(6) Jantunen, K. C.; Scott, B. L.; Kiplinger, J. L. A comparative study of the reactivity of Zr(IV), Hf(IV) and Th(IV) metallocene complexes: Thorium is not a Group IV metal after all. *J. Alloys Compd.* **2007**, *444*−*445*, 363−368.
(7) Kozimor, S. A.; Yang, P.; Batista, E. R.; Boland, K. S.; Burns, C. J.; Clark, D. L.; Conradson, S. D.; Martin, R. L.; Wilkerson, M. P.; Wolfsberg, L. E. Trends in Covalency for d- and f-Element Metallocene Dichlorides Identified Using Chlorine K-Edge X-ray Absorption Spectroscopy and Time-Dependent Density Functional Theory. *J. Am. Chem. Soc.* **2009**, *131*, 12125−12136.
(8) Neidig, M. L.; Clark, D. L.; Martin, R. L. Covalency in f-element complexes. *Coord. Chem. Rev.* **2013**, *257*, 394−406.
(9) Jones, M. B.; Gaunt, A. J. Recent Developments in Synthesis and Structural Chemistry of Nonaqueous Actinide Complexes. *Chem. Rev.* **2013**, *113*, 1137−1198.
(10) Minasian, S. G.; Boland, K. S.; Feller, R. K.; Gaunt, A. J.; Kozimor, S. A.; May, I.; Reilly, S. D.; Scott, B. L.; Shuh, D. K. Synthesis and Structure of $(Ph_4P)_2MCl_6$ (M = Ti, Zr, Hf, Th, U, Np, Pu). *Inorg. Chem.* **2012**, *51*, 5728−5736.
(11) Minasian, S. G.; Keith, J. M.; Batista, E. R.; Boland, K. S.; Clark, D. L.; Conradson, S. D.; Kozimor, S. A.; Martin, R. L.; Schwarz, D. E.; Shuh, D. K.; Wagner, G. L.; Wilkerson, M. P.; Wolfsberg, L. E.; Yang, P. Determining Relative f and d Orbital Contributions to M−Cl Covalency in MCl_6^{2-} (M = Ti, Zr, Hf, U) and $UOCl_5^-$ Using Cl K-Edge X-ray Absorption Spectroscopy and Time-Dependent Density Functional Theory. *J. Am. Chem. Soc.* **2012**, *134*, 5586−5597.
(12) Silver, M. A.; Albrecht-Schmitt, T. E. Evaluation of f-element borate chemistry. *Coord. Chem. Rev.* **2016**, *323*, 36−51.
(13) Cozzi, P. G. Metal-Salen Schiff base complexes in catalysis: practical aspects. *Chem. Soc. Rev.* **2004**, *33*, 410−421.
(14) Dame, A. N.; Bharara, M. S.; Barnes, C. L.; Walensky, J. R. Synthesis of Thorium(IV) and Uranium(IV) Salicylaldiminate Pseudo-Halide Complexes. *Eur. J. Inorg. Chem.* **2015**, *2015*, 2996−3005.
(15) Wu, W.; Sun, J.; Ji, S.; Wu, W.; Zhao, J.; Guo, H. Tuning the emissive triplet excited states of platinum(II) Schiff base complexes with pyrene, and application for luminescent oxygen sensing and triplet-triplet-annihilation based upconversions. *Dalton Trans.* **2011**, *40*, 11550−11561.
(16) Tian, Z.; Cui, S.; Liu, G.; Wang, R.; Pu, S. A new fluorescent sensor for Zn^{2+} based on diarylethene with a 4-diethylamino-salicylaldehyde Schiff base unit. *J. Phys. Org. Chem.* **2016**, *29*, 421−429.
(17) Sahraei, A.; Kargar, H.; Hakimi, M.; Tahir, M. N. Distorted square-antiprism geometry of new zirconium (IV) Schiff base complexes: Synthesis, spectral characterization, crystal structure and investigation of biological properties. *J. Mol. Struct.* **2017**, *1149*, 576−584.
(18) Gao, T.; Yan, P.-F.; Li, G.-M.; Hou, G.-F.; Gao, J.-S. Ion size dominated 1D and 2D Salen lanthanide coordination complexes and their luminescence. *Polyhedron* **2007**, *26*, 5382−5388.
(19) Yan, P.; Sun, W.; Li, G.; Nie, C.; Gao, T.; Yue, Z. Synthesis, characterization and fluorescence of lanthanide Schiff-base complexes. *J. Coord. Chem.* **2007**, *60*, 1973−1982.
(20) Gao, B.; Zhang, Q.; Yan, P.; Hou, G.; Li, G. Crystal engineering of salen type cerium complexes tuned by various cerium counterions. *CrystEngComm* **2013**, *15*, 4167−4175.
(21) Pospieszna-Markiewicz, I.; Radecka-Paryzek, W.; Kubicki, M.; Korabik, M.; Hnatejko, Z. Different supramolecular architectures in self-assembled praseodymium(III) and europium(III) complexes with rare coordination pattern of salicylaldimine ligand. *Polyhedron* **2015**, *97*, 167−174.
(22) Hardy, E. E.; Wyss, K. M.; Gorden, J. D.; Ariyarathna, I. R.; Miliordos, E.; Gorden, A. E. V. Th(IV) and Ce(IV) napthylsalophen sandwich complexes: characterization of unusual thorium fluorescence in solution and solid-state. *Chem. Commun.* **2017**, *53*, 11984−11987.
(23) Salmon, L.; Thuéry, P.; Ephritikhine, M. Synthesis and crystal structure of uranium(IV) complexes with compartmental Schiff bases: from mononuclear species to tri- and tetranuclear clusters. *Dalton Trans.* **2004**, *10*, 1635−1643.
(24) Camp, C.; Mougel, V.; Horeglad, P.; Pécaut, J.; Mazzanti, M. Multielectron Redox Reactions Involving C−C Coupling and Cleavage in Uranium Schiff Base Complexes. *J. Am. Chem. Soc.* **2010**, *132*, 17374−17377.
(25) Camp, C.; Guidal, V.; Biswas, B.; Pécaut, J.; Dubois, L.; Mazzanti, M. Multielectron redox chemistry of lanthanide Schiff-base complexes. *Chem. Sci.* **2012**, *3*, 2433−2448.
(26) He, F.-F.; Wang, H.-Q.; Wang, X.-F.; Wang, Y.-Y. Crystal structure of bis-[N,N'-bis-(3-allyl salicylidene)-o-phenylene diamine] thorium (IV), $C_{52}H_{44}N_4O_4Th$. *Z. Kristallogr.—New Cryst. Struct.* **2012**, *227*, 521−524.
(27) Stobbe, B. C.; Powell, D. R.; Thomson, R. K. Schiff base thorium(IV) and uranium(IV) chloro complexes: synthesis, substitution and oxidation chemistry. *Dalton Trans.* **2017**, *46*, 4888−4892.
(28) Camp, C.; Toniolo, D.; Andrez, J.; Pécaut, J.; Mazzanti, M. A versatile route to homo- and hetero-bimetallic 5f−5f and 3d−5f complexes supported by a redox active ligand framework. *Dalton Trans.* **2017**, *46*, 11145−11148.
(29) Frederick, J.; Wolter, H. C. D., Jr. Plutonium Compounds and Process for Their Preparation. U.S. Patent 2,819,280, 1958.
(30) Magnusson, L. B. Separation Process for Transuranic Element and Compounds Thereof. U.S. Patent 2,830,066, 1958.
(31) Chuguryan, D. G.; Struchkov, Y. T. Crystal and Molecular Structure of Uranium(VI) and Neptunium(VI) Complexes with N,N'-bis(salicylidene)ethylenediamine. *Radiokhimiya* **1988**, *30*, 39−44.
(32) Copping, R.; Mougel, V.; Den Auwer, C.; Berthon, C.; Moisy, P.; Mazzanti, M. A tetrameric neptunyl(V) cluster supported by a Schiff base ligand. *Dalton Trans.* **2012**, *41*, 10900−10902.
(33) Klamm, B. E.; Windorff, C. J.; Marsh, M. L.; Meeker, D. S.; Albrecht-Schmitt, T. E. Schiff-base coordination complexes with plutonium(IV) and cerium(IV). *Chem. Commun.* **2018**, *54*, 8634−8636.
(34) Yu, T.; Zhang, K.; Zhao, Y.; Yang, C.; Zhang, H.; Fan, D.; Dong, W. A new trinuclear zinc(II) complex possessing five- and six-coordinated central ions and its photoluminescent property. *Inorg. Chem. Commun.* **2007**, *10*, 401−403.
(35) Li, Q.; Yan, P.; Chen, P.; Hou, G.; Li, G. Salen Type Sandwich Triple-Decker Tri- and Di-nuclear Lanthanide Complexes. *J. Inorg. Organomet. Polym.* **2012**, *22*, 1174−1181.
(36) Kubono, K.; Hirayama, N.; Kokusen, H.; Yokoi, K. X-ray Crystallographic Approach to the Design of the Phenolic Schiff Base Reagents for the Mutual Separation of Lanthanoids. *Anal. Sci.* **2001**, *17*, 193−197.
(37) Gottfriedsen, J.; Spoida, M.; Blaurock, S. Synthesis and Structure of the Cerium Schiff-Base Complexes $[Ce(Salen')_2]$ and $[(THF)_2KCe(Salen')_2]$. *Z. Anorg. Allg. Chem.* **2008**, *634*, 514−518.
(38) Szłyk, E.; Wojtczak, A.; Dobrzańska, L.; Barwiołek, M. X-ray crystal structure and nuclear Overhauser effect studies of cerium(IV) complexes with Schiff bases obtained from N,N'-(1R,2R)(−)-1,2-cyclohexanediamine and benzaldehyde derivatives. *Polyhedron* **2008**, *27*, 765−776.
(39) Kiplinger, J. L.; Morris, D. E.; Scott, B. L.; Burns, C. J. Convenient Synthesis, Structure, and Reactivity of $(C_5Me_5)U(CH_2C_6H_5)_3$: A Simple Strategy for the Preparation of Monopentamethylcyclopentadienyl Uranium(IV) Complexes. *Organometallics* **2002**, *21*, 5978−5982.
(40) *APEX3*, 2017.3-0; Bruker AXS, Inc.: Madison, WI, 2017.
(41) *SAINT*, 8.30; Bruker AXS, Inc.: Madison, WI, 2012.
(42) Sheldrick, G. M. *SADABS*, 2012/1; Bruker AXS, Inc.: Madison, WI, 2012.
(43) *OLEX2*, 1.2.10; OlexSys Ltd., 2004−2018.

DOI: 10.1021/acs.inorgchem.8b02700
Inorg. Chem. XXXX, XXX, XXX−XXX

(44) Neese, F. The ORCA program system. *Comput. Mol. Biosci.* **2012**, *2*, 73−78.
(45) Sukumar, N.; Breneman, C. M. QTAIM in Drug Discovery and Protein Modeling. In *The Quantum Theory of Atoms in Molecules*; Wiley, 2007.
(46) Lu, T.; Chen, F. Multiwfn: A multifunctional wavefunction analyzer. *J. Comput. Chem.* **2012**, *33*, 580−592.
(47) Terzis, A.; Mentzafos, D.; Tajmir-Riahi, H. A. Eight-coordination. Synthesis and structure of the schiff-base chelate bis(N,N′-disalicylidene-1,2-phenylenediamino)cerium(IV). *Inorg. Chim. Acta* **1984**, *84*, 187−193.
(48) Chen, C.; Chen, H.; Yan, P.; Hou, G.; Li, G. Structure and electrochemistry of salen type cerium (IV) complexes tuned by multiform counterions. *Inorg. Chim. Acta* **2013**, *405*, 182−187.
(49) Hill, R. J.; Rickard, C. E. F. The crystal structure of bis[N,N′-o-phenylenebis(salicylaldiminato)] thorium(IV). *J. Inorg. Nucl. Chem.* **1978**, *40*, 2029−2032.
(50) Illingsworth, M. L.; Rheingold, A. L. Synthesis and molecular structure of the eight-coordinate complex bis(4-amino-N,N'-disalicylidene-1,2-phenylenediaminato)zirconium(IV), a new reagent for preparing coordination polymers. *Inorg. Chem.* **1987**, *26*, 4312−4318.
(51) Saha, T. K.; Ramkumar, V.; Chakraborty, D. Salen Complexes of Zirconium and Hafnium: Synthesis, Structural Characterization, Controlled Hydrolysis, and Solvent-Free Ring-Opening Polymerization of Cyclic Esters and Lactides. *Inorg. Chem.* **2011**, *50*, 2720−2722.
(52) Matsumoto, K.; Watanabe, A.; Uchida, T.; Ogi, K.; Katsuki, T. Construction of a new asymmetric reaction site: asymmetric 1,4-addition of thiol using pentagonal bipyramidal Hf(salen) complex as catalyst. *Tetrahedron Lett.* **2004**, *45*, 2385−2388.
(53) Shannon, R. D. Revised effective ionic radii and systematic studies of interatomic distances in halides and chalcogenides. *Acta Crystallogr., Sect. A: Found. Crystallogr.* **1976**, *32*, 751−767.
(54) Hobart, D. E.; Morris, D. E.; Palmer, P. D.; Newton, T. W. *Formation, Characterization, and Stability of Plutonium(IV) Colloid*; LA-UR-89-2541; Los Alamos National Laboratory, 1989; pp 0612−0620.
(55) Jantunen, K. C.; Burns, C. J.; Castro-Rodriguez, I.; Da Re, R. E.; Golden, J. T.; Morris, D. E.; Scott, B. L.; Taw, F. L.; Kiplinger, J. L. Thorium(IV) and Uranium(IV) Ketimide Complexes Prepared by Nitrile Insertion into Actinide−Alkyl and −Aryl Bonds. *Organometallics* **2004**, *23*, 4682−4692.
(56) Bard, J. A.; Faulkner, L. R., *Electrochemical Methods: Fundamentals and Applications*, 2nd ed.; John Wiley & Sons, Inc., 2001.
(57) Cohen, A. J.; Mori-Sánchez, P.; Yang, W. Challenges for Density Functional Theory. *Chem. Rev.* **2012**, *112*, 289−320.
(58) Cremer, D.; Kraka, E. Chemical Bonds without Bonding Electron Density — Does the Difference Electron-Density Analysis Suffice for a Description of the Chemical Bond? *Angew. Chem., Int. Ed.* **1984**, *23*, 627−628.
(59) Espinosa, E.; Alkorta, I.; Elguero, J.; Molins, E. From weak to strong interactions: A comprehensive analysis of the topological and energetic properties of the electron density distribution involving X−H···F−Y systems. *J. Chem. Phys.* **2002**, *117*, 5529−5542.
(60) Kerridge, A. f-Orbital covalency in the actinocenes (An = Th−Cm): multiconfigurational studies and topological analysis. *RSC Adv.* **2014**, *4*, 12078−12086.
(61) Beekmeyer, R.; Kerridge, A. Assessing Covalency in Cerium and Uranium Hexachlorides: A Correlated Wavefunction and Density Functional Theory Study. *Inorganics* **2015**, *3*, 482−499.
(62) Gregson, M.; Lu, E.; Tuna, F.; McInnes, E. J. L.; Hennig, C.; Scheinost, A. C.; McMaster, J.; Lewis, W.; Blake, A. J.; Kerridge, A.; Liddle, S. T. Emergence of comparable covalency in isostructural cerium(IV)− and uranium(IV)−carbon multiple bonds. *Chem. Sci.* **2016**, *7*, 3286−3297.

DOI: 10.1021/acs.inorgchem.8b02700
Inorg. Chem. XXXX, XXX, XXX−XXX